Geochemistry, Geophysics, Geosystems

RESEARCH ARTICLE
10.1029/2019GC008717

Special Section:
Slow Slip Phenomena and Plate Boundary Processes

Observations of Laboratory and Natural Slow Slip Events: Hikurangi Subduction Zone, New Zealand

Matt J. Ikari[1], Laura M. Wallace[2,3], Hannah S. Rabinowitz[4], Heather M. Savage[5], Ian J. Hamling[2], and Achim J. Kopf[1]

[1]MARUM Center for Marine Environmental Sciences and Faculty of Geosciences, University of Bremen, Bremen, Germany, [2]GNS Science, Lower Hutt, New Zealand, [3]Institute for Geophysics, University of Texas, Austin, TX, USA, [4]Department of Earth, Environmental, and Planetary Sciences, Brown University, Providence, RI, USA, [5]Department of Earth and Planetary Sciences, University of California, Santa Cruz, Santa Cruz, CA, USA

Abstract Slow slip events (SSEs) are recognized as an important component of plate boundary fault slip, and there is a need for laboratory friction data on natural samples to guide comparisons with natural SSEs. Here, we compile a comprehensive catalog of SSEs observed geodetically at the Hikurangi subduction zone offshore northern New Zealand, and compare it with results of laboratory friction experiments that produce laboratory SSEs under plate tectonic driving rates (5 cm/yr). We use samples from Ocean Drilling Program Site 1124 seaward of the Hikurangi subduction zone to represent the plate boundary that hosts shallow SSEs at Hikurangi. We find that laboratory SSEs exhibit a similar displacement record and range of stress drops as the natural SSEs. Results of velocity step tests, which can be used to evaluate frictional instability based on the critical stiffness criterion, indicate that the slow slip activity at Hikurangi is a form of stably-accelerating slip. Our laboratory SSEs provide an alternative method of quantifying (in)stability by direct measurement of the unloading stiffness during the stress drop. The observed dependence of laboratory SSE parameters on effective normal stress is consistent with critical stiffness theory; however, depth-increasing projections based on laboratory data do not match observations from natural SSEs. These differences are likely related to changing temperature and fault rock composition downdip but also complications related to scaling and/or limited sampling. Scientific drilling recently undertaken at the Hikurangi subduction zone should serve to improve and guide future studies of the role of frictional properties for the occurrence of SSEs.

Key Points:
- We compare laboratory-observed slow slip events with a complete catalog of natural slow slip events in Hikurangi, New Zealand
- Natural and laboratory slow slip events share some similarities, but extrapolation from the laboratory to the field remains problematic
- For laboratory SSEs, critical stiffness derived from stress drops predicts fault behavior better than parameters extracted from velocity step tests

Supporting Information:
- Supporting Information S1
- Figure S1
- Figure S2
- Table S1

Correspondence to:
M. J. Ikari,
mikari@marum.de

Citation:
Ikari, M. J., Wallace, L. M., Rabinowitz, H. S., Savage, H. M., Hamling, I. J., & Kopf, A. J. (2020). Observations of laboratory and natural slow slip events: Hikurangi subduction zone, New Zealand. *Geochemistry, Geophysics, Geosystems*, *21*, e2019GC008717. https://doi.org/10.1029/2019GC008717

Received 20 AUG 2018
Accepted 6 JAN 2020
Accepted article online 26 JAN 2020

1. Introduction

Although slow fault slip events have been observed for decades (e.g., Goulty & Gilman, 1978; Ihmlé & Jordan, 1994; Linde et al., 1988; Sacks et al., 1978, 1981), improved and widespread geodetic observations have rapidly increased understanding of these phenomena over the past ~20 years. Slow and transient fault slip occurs over a wide range of timescales, from long-term slow slip events (SSEs) with durations on the order of years, to low-frequency earthquakes that are fast enough to be detected seismologically (Ide et al., 2007; Peng & Gomberg, 2010). SSEs are considered important due to their impact on the seismic cycle; however, the exact nature of the relationship between slow slip and seismic slip is unclear. In some cases, SSEs are thought to increase earthquake hazard by loading adjacent fault patches (Kaneko et al., 2018; Koulali et al., 2017; Mazzotti & Adams, 2004; Reyners & Bannister, 2007; Wech & Creager, 2011). Earthquakes can also trigger SSEs (Wallace et al., 2017, 2018) even if the triggering earthquake is small (Han et al., 2014); conversely, they can also arrest SSEs (Wallace et al., 2014). The location of SSEs in some subduction zones suggests that they delineate locked zones, perhaps revealing the region of future coseismic ruptures (Chapman & Melbourne, 2009; Dixon et al., 2014; Wallace & Beavan, 2010). In other cases, they can occur on the seismogenic portion of the subduction megathrust (Ito et al., 2013; Larson et al., 2007; Ruiz et al., 2014). One particular region with well-documented SSEs is the Hikurangi subduction zone offshore New Zealand, which is the focus of this study.

The variability of SSEs and their complex relationship with ordinary earthquakes has prompted discussion on the mechanisms and conditions for SSE occurrence (e.g., Saffer & Wallace, 2015). Laboratory measurements of fault frictional properties are an essential component of studies targeting fault slip behavior. Measuring how the frictional strength of a fault depends on the slip velocity provides an indication as to

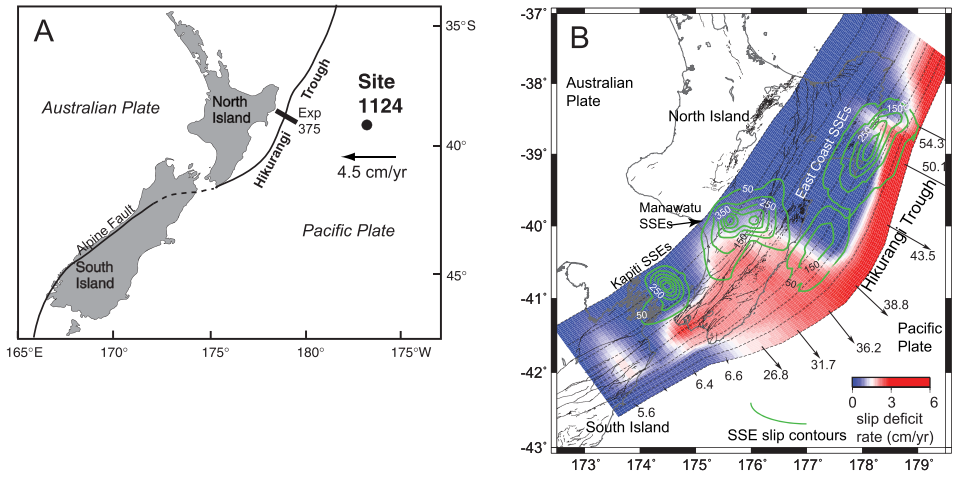

Figure 1. (a) Map of New Zealand, showing the Hikurangi margin and location of ODP Site 1124 (modified from Carter et al., 1999). Thick line shows the location of transect for drilling, coring, and observatory installation during IODP Expedition 375 (Wallace et al., 2019). (b) Red to blue colors show the degree of interseismic locking on the Hikurangi subduction thrust, and green contours denote slip in past SSEs (Wallace et al., 2012). Black arrows show motion of the overriding plate relative to the Pacific Plate at the Hikurangi trench (mm/yr).

whether a fault will slide stably or unstably, with unstable faults expected to produce ordinary earthquakes (e.g., Dieterich, 1986; Dieterich & Kilgore, 1996; Marone, 1998; Scholz, 2002). Based on this framework, SSEs are proposed to be related to the transition between unstable and stable frictional regimes (e.g., Lowry, 2006; McCaffrey et al., 2008; Rubin, 2008). A recent experimental development is the ability to shear samples at geologically realistic driving rates of cm/yr, simulating the natural driving rate boundary condition of plate-boundary faults (Ikari, Ito, et al., 2015; Ikari & Kopf, 2017). These experiments have revealed that at tectonic plate rates, spontaneous perturbations in stress and slip rate occur that resemble geodetic observations of natural SSEs. This facilitates comparison between natural and laboratory SSEs, and measurements of frictional properties may provide insight into the mechanism behind SSEs.

Here, we present the results of laboratory friction experiments utilizing driving velocities as low as 5 cm/yr, conducted on a sample of sediment recovered from the subducting plate ~400 km east of the Hikurangi subduction margin. The lithologic unit is typical of the incoming sediment section and is likely representative of the shallow decollement at the northern Hikurangi subduction margin, where seafloor geodetic studies have documented SSEs to within at least 2 km of the seafloor (Wallace et al., 2016). We compare characteristics of natural SSEs in the Hikurangi region with observations from laboratory SSEs, with the goal of constraining the mechanism of natural SSEs, and providing a first step toward linking laboratory and observational data sets.

2. Hikurangi Subduction Zone, New Zealand

The Hikurangi subduction zone is located off the east coast of New Zealand's North Island (Figure 1). It is formed by westward subduction of the Pacific plate at a rate of 2–6 cm/yr (Wallace et al., 2004). This margin has hosted megathrust earthquakes with moment magnitude M_w of up to 7.1, but none larger over the past century (Doser & Webb, 2003). However, indications of geodetic locking (Figure 1b) suggest that the plate interface could rupture in earthquakes of M_w 8 or larger (Wallace et al., 2009).

Notably, this region is one of the best studied examples of a subduction zone that hosts frequent SSEs, which have been detected geodetically since 2002 by a continuous Global Positioning System (cGPS) network (Bartlow et al., 2014; Douglas et al., 2005; McCaffrey et al., 2008; Wallace et al., 2009, 2012, 2014, 2016, 2018, 2017; Wallace & Beavan, 2006, 2010; Wallace & Eberhart-Phillips, 2013). A striking characteristic of the Hikurangi SSEs is the clear separation at ~40–41°S between shallow SSEs (<15 km depth) in the northern Hikurangi Trench, and deeper SSEs (~30–60 km depth) to the south (Figure 1b; Tables 1 and 2). In general, the shallower events are shorter (2–3 weeks) and more frequent (every 1–2 years), while deep events are

Geochemistry, Geophysics, Geosystems

10.1029/2019GC008717

Table 1
Northern Hikurangi SSE parameters

Event and Year	Duration (Days)	Depth of Maximum Slip (km)	Maximum Slip D (mm)	Stress Drop (kPa)	Peak Slip Velocity V (cm/yr)	Event V/Vo	Downdip Width (km)	D/r	Mw	Reference
Gisborne Nov 2004	17	12.0	180	51.7	386.5	193.2	46	7.8E-06	6.3	Wallace & Beavan, 2010
Tolaga Bay Dec 2004	20	3.5	40	1.4	73.0	36.5	93	8.6E-07	6.0	Wallace & Beavan, 2010
S. Hawkes Bay June 2006	7	12.0	40	1.9	208.6	104.3	72	1.1E-06	6.1	Wallace & Beavan, 2010
Gisborne July 2006	6	12.0	40	2.8	243.3	121.7	87	9.2E-07	6.3	Wallace & Beavan, 2010
S. Hawkes Bay August 2006	7	9.6	220	19.2	1147.1	573.6	81	5.4E-06	6.6	Wallace & Beavan, 2010
N. of Gisborne Dec 2007	34	10.0	90	6.2	96.6	48.3	62	2.9E-06	6.2	Wallace & Beavan, 2010
S. Hawkes Bay March 2008	5	12.0	30	1.6	219.0	109.5	52	1.1E-06	6.1	Wallace & Beavan, 2010
Mahia Mar 2008	15	12.8	85	4.5	206.8	103.4	78	2.2E-06	6.4	Wallace & Beavan, 2010
Tolaga Bay Aug 2008	12	9.0	45	3.3	136.9	68.4	61	1.5E-06	6.1	Wallace & Beavan, 2010
Tolaga Bay + Mahia Feb 2010	14	9.0	120	7.4	312.9	156.4	84	2.9E-06	6.4	Wallace & Beavan, 2010
Gisborne March 2010	16	13.0	125	8.8	285.2	142.6	70	3.6E-06	6.4	Wallace & Beavan, 2010
Cape Turnagain 2011	32	9.6	100	5.1	114.1	57.0	105	1.9E-06	6.5	Wallace et al., 2012
Hawkes Bay 2011	20	15.0	40	3.3	73.0	36.5	65	1.2E-06	6.1	Wallace et al., 2012
Tolaga Bay 2011	21	12.0	60	6.7	104.3	52.1	36	3.3E-06	5.9	Wallace et al., 2012
Gisborne 2011	11	12.0	55	4.3	182.5	91.3	66	1.7E-06	6.2	Wallace et al., 2012
Hawkes Bay/Cape Turnagain 2013	12	9.0	240	15.1	730.0	365.0	91	5.3E-06	6.5	Wallace & Eberhart-Phillips, 2013
Tolaga Bay 2013	20	9.0	150	15.2	273.8	136.9	52	5.8E-06	6.2	L. Wallace unpublished data
Gisborne 2014	24	7.0	270	21.7	410.6	205.3	33	1.6E-05	6.5	Wallace et al., 2016
East Coast triggered SSE 2016	14	7.5	130	1.5	338.9	169.5	92	2.8E-06	6.8	Wallace et al., 2017

Stress drop and M_w calculated assuming a shear modulus of 10 GPa. V_o = 2.0 cm/yr, r = half the downdip width.
Vo = initial slip velocity (cm/yr), r = downdip half width (km), Mw = moment magnitude

Geochemistry, Geophysics, Geosystems

10.1029/2019GC008717

Table 2
Southern Hikurangi SSE parameters

Event (Stage) and Year	Duration (Days)	Depth of Maximum Slip (km)	Maximum Slip D (mm)	Stress Drop (kPa)	Peak Slip Velocity V (cm/yr)	Event V/Vo	Downdip Width (km)	D/r	Mw	Reference
Kapiti 2003	202	53	200	111.3	36.1	24.1	48	8.3E-06	6.6	Wallace & Beavan, 2010
Manawatu 2004 (stage 1)	365	53	230	55.8	23.0	15.3	97	4.7E-06	6.9	Wallace & Beavan, 2010
Manawatu 2004 (stage 2)	60	50	200	39.6	121.7	81.1	104	3.8E-06	6.9	Wallace & Beavan, 2010
Manawatu 2004 (stage 3)	120	50	190	43.5	57.8	38.5	89	4.3E-06	6.8	Wallace & Beavan, 2010
Manawatu 2004 total	***545***								***7.2***	
Kapiti 2008 (stage 1)	120	53	80	26.4	24.3	16.2	48	3.4E-06	6.3	Wallace & Beavan, 2010
Kapiti 2008 (stage 2)	60	53	270	128.7	164.3	109.5	69	7.9E-06	6.7	Wallace & Beavan, 2010
Kapiti 2008 (stage 3)	90	38	110	32.1	44.6	29.7	73	3.0E-06	6.6	Wallace & Beavan, 2010
Kapiti 2008 (stage 4)	180	38	60	24.6	12.2	8.1	60	2.0E-06	6.4	Wallace & Beavan, 2010
Kapiti 2008 total	***450***								***7.0***	
Manawatu 2010/11 (stage 1)	90	53	55	11.1	22.3	14.9	81	1.4E-06	6.5	Wallace et al., 2012
Manawatu 2010/11 (stage 2)	120	38	160	31.8	48.7	32.4	95	3.4E-06	6.9	Wallace et al., 2012
Manawatu 2010/11 (stage 3)	240	38	90	23.1	13.7	9.1	83	2.2E-06	6.7	Wallace et al., 2012
Manawatu 2010/11 total	***450***								***7.1***	
Kapiti 2016 (still ongoing)	*300*	*45*	*220*	53.7	*26.8*	17.8	*88*	*5.0E-06*	*6.9*	Wallace et al., 2018

Stress drop and M_w calculated assuming a shear modulus of 30 GPa. V_o = 1.5 cm/yr, r = half the downdip width.
Vo = initial slip velocity (cm/yr), r = downdip half width (km), Mw = moment magnitude

longer (>1 year), and less frequent (recurrence of ~5 years) (Wallace et al., 2009, 2012; Wallace & Beavan, 2010). The difference in depths of occurrence for shallow and deep SSEs coincides with the depth of geodetic plate locking along the margin. The shallow SSEs largely occur at the mostly creeping (e.g., decadal scale creep, or averaged over multiple SSE cycles) northern and central Hikurangi margin, while the deep SSEs wrap around the large, locked seismogenic zone at southern Hikurangi (Figure 1b).

Geophysical logging, coring, and observatory installations were recently undertaken along a transect of drill sites spanning the Hikurangi plate boundary in late 2017 and early 2018 during IODP Expeditions 372 and 375 (Wallace et al., 2019). Prior to these expeditions, scientific drilling in this region was limited to the sedimentary sequence on the subducting Pacific plate (~400 km east of the Hikurangi Trough) that was drilled during ODP Leg 181, at Site 1124 (Carter et al., 1999). Although the goals of Expedition 181 did not focus on plate-boundary fault behavior, the incoming sediments at subduction zones are expected to be similar to those which constitute the shallow megathrust fault and are thus a valuable resource for investigating the mechanical behavior of the shallow plate boundary (e.g., Hüpers et al., 2017; Ikari et al., 2018; Underwood, 2007). The sample we use is a mixture of three core samples (20X-5, 21X-5, and 22X-5) from Site 1124, which span a recovery depth from ~195 to 215 meters below seafloor (mbsf); this is the same sample used in a recent friction study by Rabinowitz et al. (2018). Lithologically, all three samples are described as a clay-bearing nannofossil chalk with mudstone interbeds, which is generally representative of the majority of the sediment column recovered at Site 1124 (Carter et al., 1999). Following the method described in Vogt et al. (2002), the mineral assemblage of our aggregate sample was quantified by X-ray diffraction to be 43% calcite, 24% quartz+feldspar, and 20% phyllosilicates (Rabinowitz et al., 2018). Most of the phyllosilicates (8% of the bulk sediment) are mixed-layer clays, with the remaining 12% being an evenly distributed combination of smectite, illite, muscovite, kaolinite and chlorite.

3. Experimental Methods

Our sample was tested as powdered gouge (grain size <125 μm), mixed with 3.5% NaCl brine to form a stiff paste, which we cold-pressed into a sample cell that holds a cylindrical volume of ~20 mm height and 25 mm diameter. We conducted laboratory shear experiments in a single-direct shear device, within which the bottom half of the sample cell is displaced relative to the top half inducing planar shear perpendicular to the cylinder axis (see Ikari, Ito, et al., 2015). The apparatus is equipped with two independent displacement sensors in the shear direction; one mounted at the load cell monitors the apparatus driving (i.e., load point displacement), and one directly at the sample cell measures the true displacement of the sample. Our experiments were conducted at room temperature under fluid-saturated conditions; the sample is confined by the cell and porous metal plates but is not sealed and is allowed to communicate with the pore fluid reservoir. Under application of the normal stress, we allowed the sample to consolidate and drain to the open atmosphere for at least 18 hr, until the sample height (~15–20 mm) reached a steady value. Therefore, although we do not directly measure pore pressure we assume that the sample is drained before shearing and that the applied normal stress is the effective normal stress (σ_n').

We sheared our sample under σ_n' ranging from 1 up to 15 MPa, the in situ conditions for shallow slow slip at 0.2–3 km depth assuming a vertical effective stress gradient of ~5 MPa/km. Our stress gradient assumes fluid pressure in excess of hydrostatic, as is thought to occur at the northern Hikurangi margin (Bell et al., 2010; Ellis et al., 2015) and in other shallow SSE regions (Kitajima & Saffer, 2012; Saffer & Wallace, 2015). At each effective normal stress, we continuously recorded the shear strength (τ) and calculate the (apparent) coefficient of sliding friction as $\mu = \tau/\sigma_n'$. We sheared the sample at a constant displacement (or slip) rate V of 10 μm/s for up to ~4–5 mm, then decreased the driving rate to 1.7 nm/s (5 cm/yr) for ~2 mm to simulate naturally slow plate tectonic driving rates (Figure 2). We measure the stress drop, event slip, peak slip velocity, and unloading stiffness for the laboratory SSEs generated during the plate rate experiments. The driving velocity was then increased to 5.1 nm/s to measure the rate- and state-dependence of friction (RSF) using established inverse modeling techniques (Ikari et al., 2009; Reinen & Weeks, 1993; Saffer & Marone, 2003) (Figure 2).

The frictional response to a velocity step is described by the following relations:

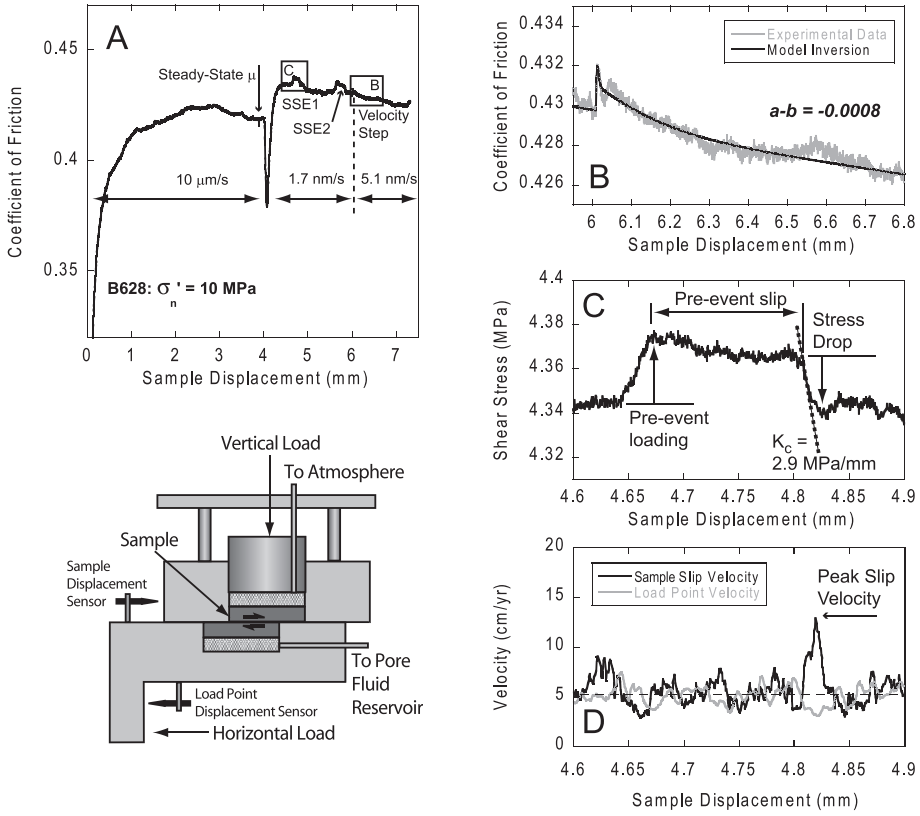

Figure 2. Example of experimental data from experiment B628 (see Rabinowitz et al., 2018), conducted at 10 MPa. (a) Coefficient of friction as a function of sample displacement, showing measurement of steady-state frictional strength, two laboratory SSEs, and a velocity-step test. (b) Close-up of the velocity step data in (a), overlain by an inverse model. Value of *a*-*b* from the model inversion is−0.0008. (c) Close-up of the first SSE indicated in (a) with shear stress shown as a function of slip, showing measurement of the event stress drop and the unloading stiffness during the stress drop, taken to be the critical stiffness K_s. (d) Same displacement range as in (c) showing the peak in sample slip velocity coinciding with the stress drop. The absence of an increase in load point velocity confirms that the slip event occurs in the sample and is not an artifact of the apparatus. Dashed line indicates the input driving velocity of 5 cm/yr. Inset below panel (a) shows a schematic diagram of the direct shear apparatus.

$$\mu = \mu_o + a\ln\left(\frac{V}{V_o}\right) + b_1\ln\left(\frac{V_0\theta_1}{d_{c1}}\right) + b_2\ln\left(\frac{V_o\theta_2}{d_{c2}}\right), \tag{1}$$

$$\frac{\mathrm{d}\theta_i}{\mathrm{d}t} = 1 - \frac{V\theta_i}{d_{ci}}, i = 1, 2 \tag{2}$$

where a, b_1, and b_2 are dimensionless constants, θ_1 and θ_2 are state variables (units of time), and d_{c1} and d_{c2} are critical slip distances over which friction evolves to a new steady state value (e.g., Dieterich, 1979, 1981; Marone, 1998; Scholz, 2002). One or two state variables may be used to describe the data as necessary.

Equation (2) describes the time-dependent evolution of the state variable θ and is known as the "Dieterich" or "slowness" law, which has the property that friction can change as a function of time and not only slip. Another well-known law used to describe the evolution of the state variable dictates that friction can change only if slip occurs and, accordingly, is called the slip law (Ruina, 1983). For certain cases such as large velocity perturbations, some studies show that the slip law better describes laboratory data (e.g., Bhattacharya et al., 2015), but for the small velocity increases we employ here that the two laws provide nearly identical results. For both state evolution laws, at steady state $\mathrm{d}\theta/\mathrm{d}t = 0$ and equations (1) and (2) simplify to

$$a-b = \frac{\Delta\mu_s}{\Delta lnV}, \tag{3}$$

where μ_s is a steady-state value of friction and $b = b_1 + b_2$. A negative value of $a - b$ corresponds to velocity-weakening friction and indicates the possibility of unstable slip, whereas materials exhibiting positive $a - b$ values (or velocity-strengthening friction) are expected to slide stably (e.g., Dieterich, 1986; Dieterich & Kilgore, 1996; Scholz, 1998).

The occurrence of unstable slip, which results in earthquakes in nature and stick-slip behavior in the laboratory, depends on a competition between the unloading stiffness (stress drop/slip) of the fault K_c and the elastic stiffness of the surroundings K, where K is the stiffness of the testing apparatus (or host rock in nature) (Cook, 1981). If the stress is relieved faster on the fault compared to its surroundings (i.e., $K < K_c$), an energy imbalance will occur which drives the slip instability (Dieterich, 1986; Dieterich & Kilgore, 1996; Rice & Ruina, 1983; Scholz, 1998, 2002). K_c is determined from RSF parameters, although we will later discuss an alternative method for determining K_c. In terms of RSF parameters, the condition for slip instability is (Gu et al., 1984)

$$K<K_c = \frac{(b-a)\sigma_n^{'}}{d_c}. \tag{4}$$

For simplicity, we assume that d_c is d_{c1} from equations (1) and (2). It can be seen from equation (4) that a velocity-strengthening material (where $b - a < 0$) makes the condition $K < K_c$ impossible, so that instability should not occur.

Equation (4) is the criterion for true slip instability, defined as the ability for the slip velocity to accelerate uninhibited toward infinity (e.g., Dieterich, 1986; Ruina, 1983). However, the RSF formulation using the Dieterich evolution law can also produce accelerating slip in velocity-strengthening materials, although it cannot continue to infinity. In this case, the critical stiffness criterion is

$$K<K_b = \frac{b\sigma_n^{'}}{d_c} + \frac{T}{V_i} \tag{5}$$

where T is an external shear stressing rate $d\tau/dt$ and V_i is the initial slip velocity (Dieterich, 1992). Assuming that the external stressing rate T is zero (i.e., the shear stress on the fault is approximately constant), it can be seen that this criterion is similar to the criterion for full instability, but with the critical stiffness depending on the parameter b rather than $a - b$. As noted by Dieterich (1992), instabilities nucleating according to this criterion may be expected to have quite limited slip, because the velocity-strengthening property will tend to damp the instability and stabilize slip. The second term on the right-hand side of equation (5) also suggests that external stress perturbations could be an important triggering mechanism especially since initial slip rates can be quite low, but we do not investigate this further in this study.

The stiffness K of our apparatus was measured by loading a steel blank the same size as our samples at a rate of 5 kPa/s under 1, 5, 10, and 15 MPa normal load, up to shear loads corresponding to a friction coefficient of at least 0.6 (well exceeding the range of friction coefficients in this study). For the observations in this study, stiffness values which matched the relevant testing conditions range from ~2–9 MPa/mm depending on the normal and shear loads. We use a critical stiffness analysis to test whether the characteristics of laboratory SSEs are consistent with the classification as frictional instabilities, and furthermore how well laboratory tests (i.e., velocity-step tests) can predict such behavior.

4. Observations From Laboratory Friction Experiments

4.1. Laboratory SSEs

The steady-state friction coefficient of the Hikurangi sediment is consistently 0.36–0.43 at the initial slip rate of 10 μm/s, and 0.41–0.45 at the slow rate of 1.7 nm/s over all effective normal stresses in this study. In five of our seven experiments, we observe 2–3 SSEs which appear spontaneously during the ~2 mm of sliding under plate-rate driving at 1.7 nm/s (Figure 2 and supporting information). Laboratory SSEs were observed at each effective normal stress in this study (Figure 2). In general, the laboratory SSEs exhibit the following

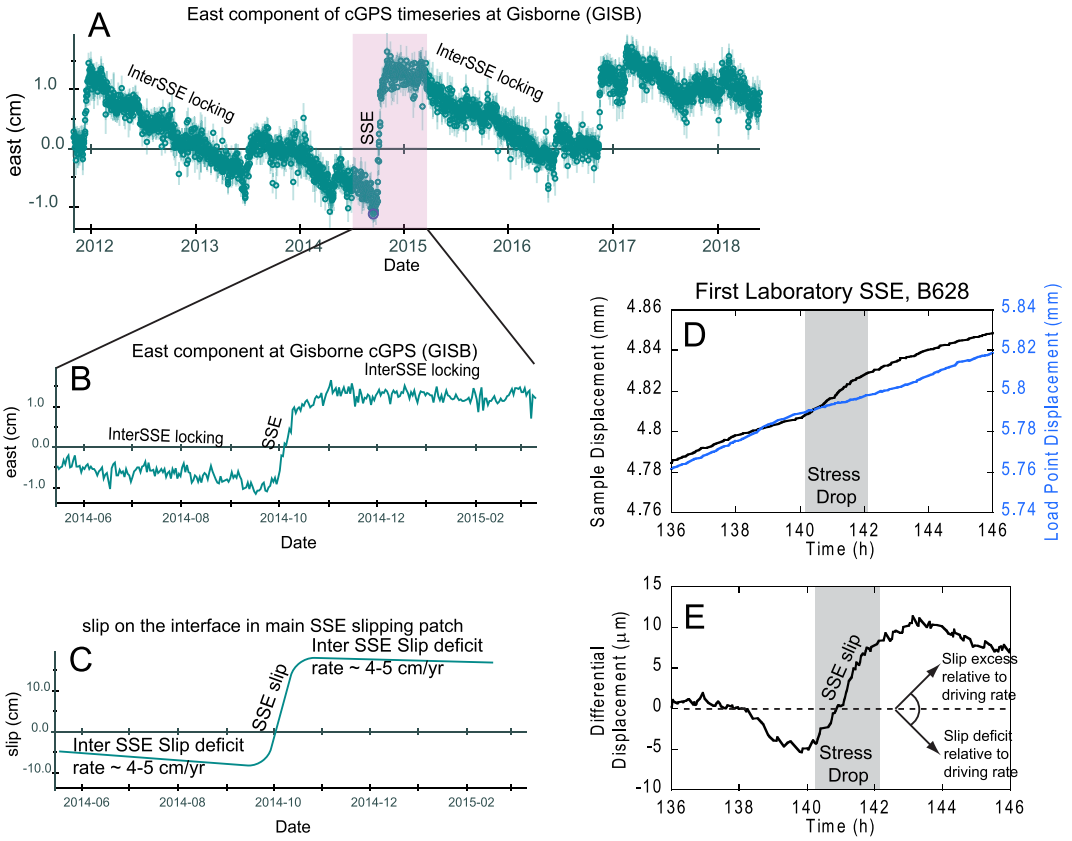

Figure 3. Comparison of geodetically measured displacement during the 2014 Gisborne SSE (Wallace et al., 2016) with a laboratory SSE (SSE1 in Figure 2). (a) Position record at cGPS station GISB, showing clear eastward motion during a SSE in in late 2014 (as well as for other smaller SSEs during the 2012–2018 period). (b) Close-up of eastward motion of station GISB, and (c) fault slip estimated on the plate interface in a region of maximum slip during the 2014 SSE (based on inversion of surface geodetic displacements, Wallace et al., 2016). (d) Displacement record of laboratory SSE1 from experiment B628. Both the sample displacement and load point (driving) displacement are shown for comparison. Note the increase in sample (but not load point) displacement at the time of the SSE stress drop. (e) Differential displacement, calculated as the difference between the sample and load point displacements, showing slip excess occurring during the SSE. A positive slope indicates excess slip relative to the driving rate, and a negative slope indicates a slip deficit relative to the driving rate. Zero slope indicates that the sample displacement matches the driving displacement.

characteristics: upon initial shearing at the driving rate, the shear stress increases signifying partial locking and slip deficit accumulation. This is followed by a stress drop of roughly equal magnitude to the loading and a simultaneous increase in sample slip rate above the programmed driving rate (i.e., sample displacement minus load point displacement), which we identify as the SSE itself. In some (but not all) SSEs, there is a phase of significant steady or quasi steady state slip between the loading phase and stress drop (Figure 2). After the SSE stress drop, the slip rate returns to the driving rate.

In Figure 3, we compare a geodetically detected natural SSE from the northern Hikurangi margin with a laboratory SSE. Shown as an example is the cGPS position record from station GISB during the 2014 Gisborne SSE (Wallace et al., 2016). Between SSEs, the time series shows a general westward motion along the direction of Pacific Plate subduction, indicating locking (or partial locking) between the plates along the subduction interface. The sudden reversal to eastward motion signifies the SSE, with a maximum of ~25 cm of slip estimated on the plate boundary fault during this particular event (Wallace et al., 2016). The form of the surface deformation response recorded by the cGPS site is very similar to the excess slip measured in laboratory SSEs, here depicted as the difference between the sample displacement and the load point displacement. Both the natural and laboratory SSEs show a trend of accumulating slip deficit before the slip event, a relatively sudden accumulation of slip, and a return to slip deficit accumulation following the event. A

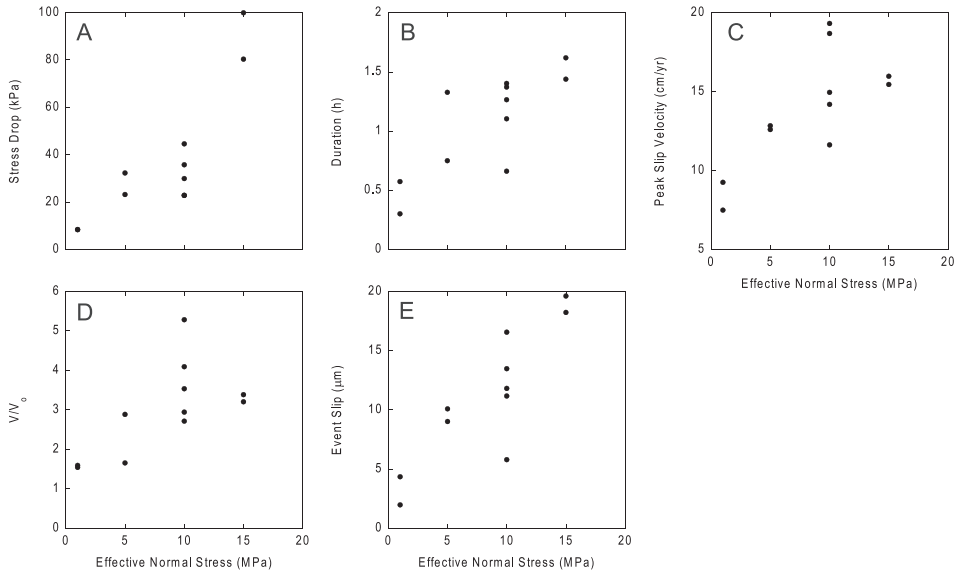

Figure 4. Measurements from laboratory SSEs: (a) stress drop, (b) duration, (c) sample peak slip velocity, (d) slip velocity increase V/V_o, and (e) sample slip as a function of effective normal stress.

point of difference to note in Figure 3c is that for the Gisborne SSE, the total slip on the plate boundary (at the point of maximum slip) is shown, whereas the slip in the laboratory SSE in Figure 3e is the excess slip (e.g., the slip beyond the steady plate motion rate). It is also important to note that the plate boundary prior to the 2014 Gisborne SSE is mostly locked and accumulating strain at nearly the full plate motion rate, whereas the sample prior to the laboratory SSE is deforming at roughly half the driving rate.

Although slip and slip velocity during the stress drop portion of the laboratory SSEs is strikingly similar to the cGPS records of natural Hikurangi SSEs (compare Figures 3a and 3e), there are also some clear differences. One is the regular, repetitive nature of the natural SSEs, which is not established in these laboratory experiments. Another difference is the steady shearing at the driving rate in the experiments, which occurs before the loadup and after the stress drop, and sometimes between the loadup and stress drop. Because such a large amount of steady shearing may not be representative of some natural slow slip faults (many of which relock quickly after an SSE, with little to no slip between SSEs), the key parameters from the laboratory SSEs (stress drop, duration, peak slip velocity, slip, and unloading stiffness) were measured specifically from the stress drop portion of the laboratory SSE. This is the part of the experimental data which most closely resemble natural SSE slip behavior (Figure 3).

For our complete set of laboratory SSEs, we observe stress drops in the range 8–100 kPa, durations of ~0.5–1.5 hr, peak slip velocities in the range 8–19 cm/yr, velocity increases (as quantified by V/V_o) of 1.5–5.3, and event slip of 2–20 μm (Figure 4, Table 3). Despite some instances of significant scatter, the stress drop, duration, peak slip velocity, slip velocity increase, and event slip all generally increase as a function of increasing effective normal stress (Figure 4). Other measurable parameters such as percent stress drop, steady-state slip preceding the stress drop, and absolute strengths prior to and after the stress drop do not show recognizable patterns as a function of effective normal stress (see supporting information).

4.2. Velocity-Dependent Frictional Behavior

From our velocity step tests for which velocity is increased from the plate rate of 1.7 nm/s, we observe velocity-weakening friction ($a - b = -0.0019$ to -0.0003) at all effective normal stresses with the exception of 5 MPa ($a - b = 0.0006$) (Figure 5). RSF parameters obtained from velocity step tests can be used to guide expectation of slow or fast slip behavior via the critical stiffness criterion (equation (4)) (e.g., Ikari, Trütner, et al., 2015; Niemeijer & Vissers, 2014; Trippetta et al., 2017). An important, but subtle point to consider is that equation (4) uses the parameter $a - b$, which includes a term for the velocity change (equation (3)). Therefore, this critical stiffness criterion is specifically applicable to the velocity changes employed in the

Table 3
Experimental SSE parameters

Experiment	Effective Normal Stress (MPa)	Stress Drop (kPa)	Event Slip D (mm)	Initial Velocity (cm/yr) Slip Vo	Peak Velocity (cm/yr) Slip V	Event V/Vo	D/r	Apparatus Stiffness K (MPa/mm)	SSE Stiffness Ks (MPa/mm)	K/Ks
B659	1	8.3	4.3	6.0	9.2	1.5	3.4E-04	8.2	2.2	1.0
B659	1	8.3	2.0	4.7	7.5	1.6	1.5E-04	8.9	3.5	0.7
B669	5	23.2	10.1	7.6	12.6	1.7	7.9E-04	2.3	2.8	2.2
B669	5	32.2	9.0	4.4	12.8	2.9	7.1E-04	2.4	4.5	1.5
B628	10	22.7	16.5	2.8	14.9	5.3	1.3E-03	9.1	2.5	3.2
B628	10	22.8	13.5	4.8	14.2	2.9	1.1E-03	8.7	2.5	3.6
B678	10	35.7	5.8	5.3	18.7	3.5	4.5E-04	6.3	13.7	0.7
B678	10	29.9	11.2	4.7	19.3	4.1	8.8E-04	6.5	3.1	2.9
B678	10	44.5	11.8	4.3	11.6	2.7	9.3E-04	8.9	8.0	1.1
B668	15	99.9	19.6	4.7	16.0	3.4	1.5E-03	8.9	8.2	1.1
B668	15	80.3	18.2	4.8	15.4	3.2	1.4E-03	8.9	7.8	1.1
B718	10	*no SSE*								
B681	15	*no SSE*								

r = 12.7 mm
Vo = initial slip velocity (cm/yr), r = sample radius (mm)

velocity step test, which in our case is $V/V_o = 3$. However, direct measurement of the velocity change during our laboratory SSE reveal V/V_o of 1.5–5.3 (Table 3). In order to directly compare K_c and K/K_c values from laboratory SSEs with K_c and K/K_c values calculated from RSF parameters, we multiply equation (4) by $\Delta \ln V_{SSE}$, which describes the change in slip rate during laboratory SSEs. We also use this factor to calculate K/K_b, the criterion for accelerating stable slip. Note that the critical slip distance d_c is implicitly assumed to be unaffected by variations in the velocity change. Since we use threefold increases in velocity for each of our velocity step tests, we cannot evaluate the effect of velocity increase magnitude on d_c. However, recent experiments using a clay-bearing synthetic gouge suggest that for velocity steps conducted at ≤1 mm/s, d_c does not vary greatly for velocity changes of up to 4 orders of magnitude (Ito & Ikari, 2015).

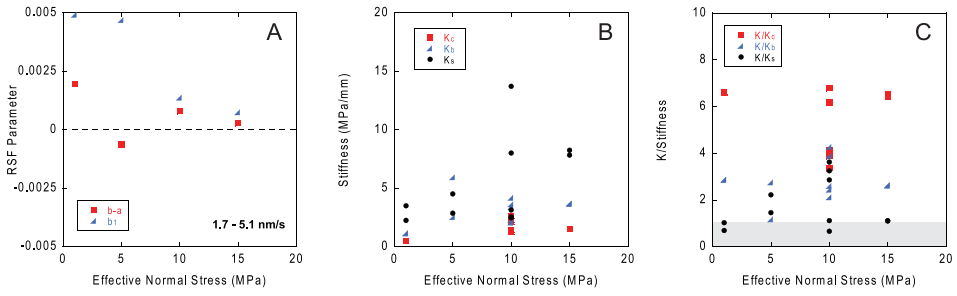

Figure 5. (a) Velocity-dependence of friction a-b, (b) critical stiffnesses K_c, K_b, and K_s, and (c) stiffness ratios K/K_c, K/K_b, and K/K_s as a function of effective normal stress. K_c is either measured directly from the slope of the stress versus displacement record during laboratory SSE (black circles), or calculated from velocity step data (blue triangles). Apparatus stiffness K = 2–9 MPa/mm (see Table 3).

The values of K_c that we obtain from our velocity step data and equation (4) range from 0.5 to 2.6 MPa/mm; K_b values are consistently larger and range from 1.1 to 5.9 MPa/mm (Figure 5). Neither K_c nor K_b exhibit a dependency on effective normal stress. For the experiment conducted at 5 MPa, K_c is a physically impossible negative value due to a measured positive $a - b$ value; K_b, values, on the other hand, can be calculated and evaluated. The stiffness of our apparatus K increases as a function of both normal and shear load. We picked K values from the loading curves to match our experimental conditions; these values range from ~2–9 MPa/mm resulting in K/K_c values ranging from 3.4–6.8. K/K_b values are smaller and range from 1.2–4.3. Although the K/K_b values are smaller and approach 1, values <1 are not observed which indicates a frictionally stable material (Figure 5).

Because we observe SSEs with clear stress drops in our laboratory experiments, we can also evaluate the sample critical stiffness directly by measuring the slope of the shear stress-displacement record during the SSE stress drop (e.g., Figure 2c). We interpret the maximum value to be a directly-measured critical stiffness during an SSE, which we call K_s. K_s values range from 2.2–13.7 MPa/mm and result in K/K_s ranging from 0.7–3.6, with about half of the K/K_s values near or below 1 (Figure 5). K_s increases slightly as a function of effective normal stress, although this trend is obscured by some scatter at 10 MPa. K/K_s does not show a dependence on normal stress, because the slight trend in K_s is canceled out by the normal stress dependence of K.

5. Comparison of Natural and Laboratory SSEs

We now compare the characteristics of our laboratory-observed SSE with a catalog of 19 shallow and 12 deep natural SSEs observed in the Hikurangi subduction zone (Wallace et al., 2009, 2012, 2016, 2017; Wallace & Beavan, 2006, 2010; Wallace & Eberhart-Phillips, 2013) (Tables 1 and 2). We compile estimates of slip magnitude, duration, depth, slip dimensions, slip rate, moment release, and stress drop based on results of these previously published geodetic studies of Hikurangi SSEs (Tables 1 and 2). Total slip, slip velocity, and duration are extracted directly from the cGPS data. Natural SSE stress drop ($\Delta\tau$) is estimated following the energy-based approach of Noda et al. (2013), which is a robust way to obtain stress drop for models with distributed slip. To do this, shear stress change is calculated for each patch/subfault in each of the SSE slip models using the equations of Okada (1992). The energy-based stress drop (Noda et al., 2013) can be expressed as:

$\Delta\tau = \frac{\sum_{i=1}^{N} \Delta\tau_i u_i}{\sum_{i=1}^{N} u_i}$, where $\Delta\tau_i$ and u_i are the stress drop (i.e., shear stress change) and slip amounts, respectively, for each slipping patch, i. The natural SSEs have an equivalent M_w of ~6–7, assuming $G = 10$ GPa for the shallow SSEs (Table 1), and $G = 30$ GPa for the deep SSEs (Table 2), which is consistent with shear moduli estimated for these depths from global subduction earthquakes (Bilek & Lay, 1999; Geist & Bilek, 2001). We note that the estimated moment magnitudes for the shallow SSEs in Table 1 are lower than those published previously, as those studies assumed a shear modulus of 30 GPa (e.g., Wallace et al., 2012, 2016; Wallace & Beavan, 2010; Wallace & Eberhart-Phillips, 2013).

To estimate the effective normal stress in the SSE source regions we assume moderate fluid overpressure approximately halfway between hydrostatic and lithostatic, for an effective normal stress gradient of 5 MPa/km. This assumption is based on seismic reflection data indicating significantly elevated fluid pressures within the Hikurangi slow slip region (Bassett et al., 2014; Bell et al., 2010). Our range of effective normal stress for the experimental SSEs therefore projects to 0.2–3 km depth, which spans the upper region of slip in the shallow SSE area (e.g., Wallace et al., 2016). Although our laboratory experiments were conducted at effective normal stresses that correspond to much shallower depths than the Hikurangi SSEs, the increasing trends with effective normal stress we observe facilitate extrapolation of laboratory-measured SSE parameters to deeper depths. For these extrapolations we use linear and power law fits to the laboratory-measured quantities, which exhibit coefficient of determination R^2 ranging from 0.54–0.75.

The stress drops of 8–100 kPa that we observe in our experiments are comparable to but slightly higher than the stress drops of 1–52 kPa observed for shallow SSEs, and very similar to the 23–129 kPa stress drops observed for the deep SSEs (Figure 6). The observation that the deeper Hikurangi SSEs have larger stress

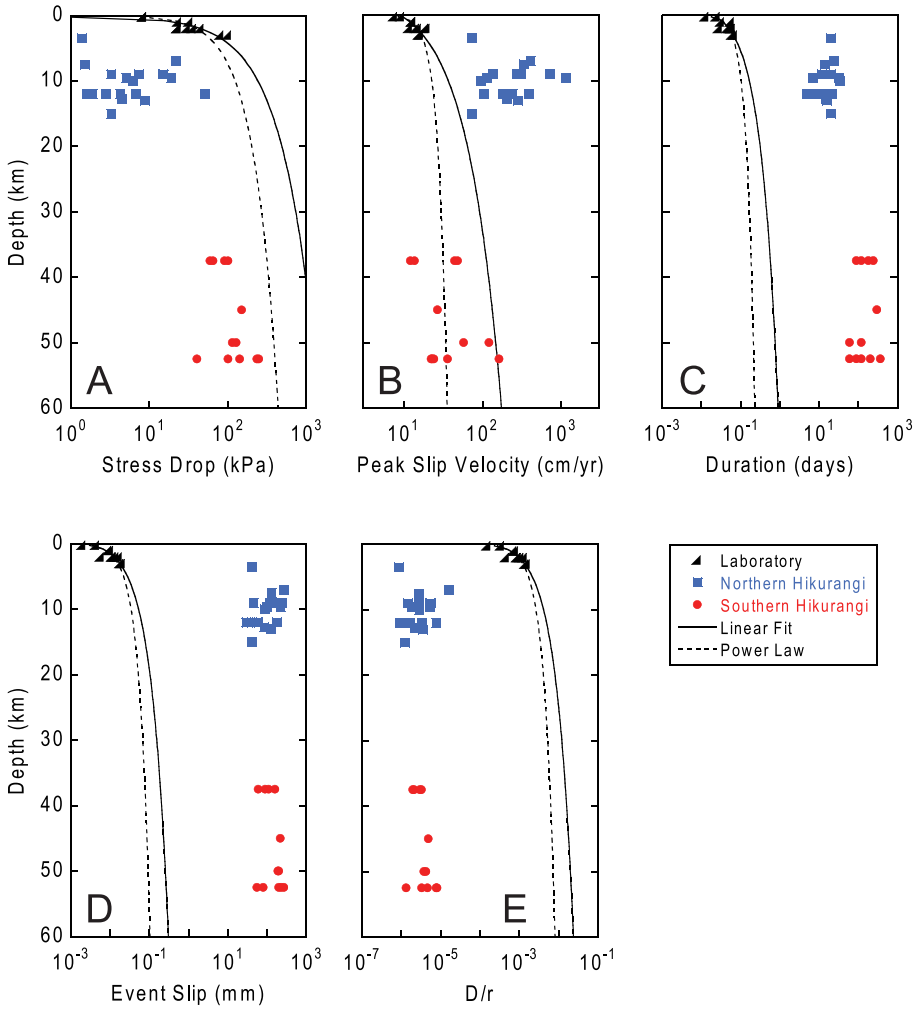

Figure 6. Comparison of parameters from laboratory SSEs with natural shallow (northern Hikurangi) and deep (southern Hikurangi) SSEs as a function of depth: (a) stress drop, (b) peak slip velocity, (c) duration, (d) event slip, and (e) slip/length ratio D/r. Effective stress gradient is assumed to be 5 MPa/km. See text for more details on SSE parameters. Linear and power law fits to the laboratory data are extrapolated to 60 km depth.

drops than the shallow SSEs is generally consistent with expectations from our laboratory data set; however, the projections overestimate the absolute stress drop values at depth. The peak slip velocities of shallow SSEs at the northern Hikurangi range from 73–1147 cm/yr (0.2–3.1 cm/day), significantly faster than both our laboratory events (8–16 cm/yr, or 0.02–0.04 cm/day), and also deep SSEs at southern Hikurangi (12–164 cm/yr or 0.03–0.45 cm/day). The shallow Hikurangi SSEs are faster than the deeper SSEs, in contrast with expectations from the laboratory SSEs. Interestingly, the depth-extrapolated peak slip velocities from the laboratory SSEs provide a good match to the deep Hikurangi SSEs (Figure 6). On the Hikurangi subduction interface the inter-SSE slip rate varies spatially and sometimes temporally, but is estimated to range from 0 (fully locked) to 3 cm/yr in the north, and 0 to 2 cm/yr in the south (Wallace & Beavan, 2010). Taking inter-SSE slip rates of 2.0 cm/yr in the northern Hikurangi and 1.5 cm/yr in the southern Hikurangi as representative, the ratio of slip velocity increase V/V_o ranges from 36 to 574 in the northern Hikurangi and 8 to 110 in the southern Hikurangi. This is significantly larger than both the twofold to fivefold increases in slip velocity measured in the laboratory SSEs, although the low values in the southern Hikurangi approach the laboratory values.

The duration of the shallow SSEs ranges from 7–34 days, and the total durations of deep events range from >300–550 days (with subevents of 60 days or more). Although the combined data set shows a trend of

increasing duration with depth as indicated by the laboratory SSEs, the durations of natural SSEs are ~2 orders of magnitude longer than the projections from the experiments (Figure 6). The maximum event slip is similar for both shallow and deep natural SSEs and ranges from ~30–300 mm. All of the natural SSEs have slip amounts that are orders of magnitude larger than those in laboratory experiments, both in terms of absolute values and the values projected to higher effective normal stresses. In order to compare between the laboratory SSEs which occur on a 500 mm^2 surface and natural SSEs with rupture dimensions of thousands of km^2, we use the dimensionless ratio D/r, where D is the maximum event slip and r is the patch half length in the slip direction (Chinnery, 1969; Dieterich, 1986). We observe that both shallow and deep SSEs have similar D/r ratios, with most values ranging from 10^{-7} to 10^{-6}. These values are approximately 2 orders of magnitude smaller than laboratory values of D/r, and approximately 3 orders of magnitude larger than the depth projections of D/r.

6. Discussion

6.1. Mechanism of Laboratory SSEs

The physical mechanisms of SSE generation are generally not well known, but SSEs can be numerically simulated by implementing velocity-weakening faults that are very close to the condition of "neutral stability" (e.g., Liu & Rice, 2005, 2007; Rubin, 2008), which is the boundary between stable sliding and unstable slip where self-sustained "stable" oscillatory motion may occur (Dieterich, 1986; Ruina, 1983; Scholz, 1998). Laboratory studies support this idea, showing that $K = K_c$, or K slightly smaller than K_c is a condition favorable for oscillatory slip that may represent SSEs (Leeman et al., 2016; Scuderi et al., 2016). Two-dimensional RSF models suggest that in order for slow slip patches to grow to the size observed in subduction zones (without overtuning of RSF parameters), additional processes are needed. One popular mechanism is an observed transition in $a - b$ from velocity weakening to velocity strengthening with increasing slip velocity, used as a mathematical cutoff that limits the slip rate (i.e., cutoff velocity) (e.g., Matsuzawa et al., 2010; Shibazaki & Iio, 2003; Shibazaki & Shimamoto, 2007). Other mechanisms for keeping slip instabilities slow include dilatancy hardening, in which dilatancy during slip causes a drop in pore pressure that strengthens the fault (Rubin, 2008; Segall et al., 2010), and geologic heterogeneity causing a distribution of velocity-weakening and velocity-strengthening fault patches (Skarbek et al., 2012). Despite the difference in mechanisms limiting the event velocity, common to all these is an initially nucleating instability at the condition $K/K_c \leq 1$ and propagation of an SSE within the rupture patch.

The K/K_c values calculated from velocity step data all exceed 1, indicating that the criterion for slip instability is not satisfied. On the other hand, many of the K/K_s values obtained from the SSE stress drops are near or sometimes below 1. Since K_s is directly measured from the SSE stress drop it is difficult to associate it with a mechanism. We note that K_s and K/K_s are more similar to the values of K_b and K/K_b, than they are to K_c and K/K_c (Figure 5). This suggests that the laboratory SSEs may be instances of accelerating stable slip. Dieterich (1992) noted that accelerating slip arising from satisfying equation (5) can occur for velocity-strengthening materials, where the velocity-strengthening property functions as a slip stabilizer. This is consistent with studies utilizing a critical slip rate above which velocity-weakening friction limits the event slip velocity. Recently, friction experiments conducted at 10 MPa effective normal stress have shown that the transition velocity for the same Hikurangi samples we use here is ~1 μm/s (Rabinowitz et al., 2018). Most of the peak slip velocities we observe (both in natural and laboratory SSEs) are at least an order of magnitude lower than 1 μm/s, perhaps suggesting that the cutoff velocity alone is unlikely to be the mechanism for Hikurangi SSEs. However, accelerating slip depends on whether the critical stiffness criterion (equation (5)) is satisfied, not necessarily if velocity-strengthening occurs. Therefore, the effect of a 1 μm/s transition velocity may be to limit natural SSEs to a maximum slip rate of ~0.1–0.4 μm/s. This inference is consistent with numerical simulations of SSEs using a 1 μm/s cutoff velocity, which show that the SSE peak slip velocities are near or sometimes lower than the cutoff velocity (Hawthorne & Rubin, 2013; Shibazaki & Shimamoto, 2007), but would need to be verified specifically for the Hikurangi margin. We emphasize that this transition velocity has thus far only been measured at 10 MPa effective normal stress on the Hikurangi samples; however, we also note that while K/K_b values approach 1, values less than 1 are not observed.

The observation of laboratory SSEs despite the critical stiffness criteria K/K_c and K/K_b not being satisfied indicates that K_s values measured directly from laboratory SSEs may be a more reliable indicator of slow

slip behavior compared to RSF parameters extracted from velocity-step data, especially in material with $a - b$ values that are positive or near 0. A similar approach was used by Harbord et al. (2017), who used stiffness values from stick-slip stress drops to reconcile the appearance of stick-slip in a velocity-strengthening material. Furthermore, although K/K_b values >1 nominally indicate stable frictional behavior, we note that it is not established what range of K/K_b values allow slow slip, that is, how close K/K_b must be to 1. Our data, which show that K/K_b from laboratory SSEs is mostly < ~3, suggest that slow events can be generated when K/K_b is slightly positive. In experiments using quartz powder in which the critical stiffness was controlled by adjusting the effective normal stress, Scuderi et al. (2016) and Leeman et al. (2016) observed that slow stick-slip mostly occurred when $K/K_c \leq 1$, but some events occurred for K/K_c up to 1.2. Their experiments therefore demonstrate that slip instability can occur even when the critical stiffness criterion is not satisfied, which we suggest may also be the case for stable accelerating slip via low K/K_b.

6.2. Differences Between Laboratory and Natural SSEs

In comparing the laboratory and natural Hikurangi SSEs, we have largely focused on SSE parameters measured during the peak slipping, or stress drop phase of the laboratory SSEs, which bear strong similarities to cGPS observations of the natural Hikurangi SSEs. However, other aspects of the laboratory SSEs are not consistent with natural SSEs. These include the steady shearing (sample slip rate about the same as the driving rate) before loadup, after the stress drop, and sometimes between the loadup and stress drop; the lack of regular recurrence of the laboratory SSEs; the spontaneous nature of partial locking represented by the loadup phase; and the short duration of the partial locking compared to steady shearing. Wallace and Beavan (2010) determined an inter-SSE locking distribution for the Hikurangi subduction interface, and the slip deficit rates in the shallow, northern Hikurangi SSE region range from 2–5 cm/yr, roughly corresponding to an inter-SSE slip rate in the SSE source of 0–3 cm/yr (where 0 is fully locked). In natural SSEs at north Hikurangi, fault locking appears to resume within a few weeks of the SSEs, and the SSE source regions there appear to largely maintain this coupling until the next SSE.

The occurrence of $K/K_b > 1$ in our experiments indicates a tendency for stable slip that could partially explain the steady shearing (sample slip rate about the same as the driving rate) before and after the stress drop, and also the lack of regular recurrence of the laboratory SSEs. We speculate that perhaps a lower K/K_b, whether from lower apparatus stiffness, higher normal load, or smaller d_c could result in more regularly repeating SSEs, larger peak slip velocities, and lower inter-SSE slip velocities that more closely resemble natural SSEs. The steady shearing before the load-up phase also indicates that our samples experience spontaneous partial locking, which is likely facilitated by the extremely low driving rates we employ here. Slow shearing may allow time-dependent frictional healing (e.g., Dieterich, 1972) to become significant even during shear, which has been suggested to favor velocity-weakening friction at low slip rates (Ikari & Kopf, 2017).

Another potentially important factor may be the role of the critical slip distance d_c. Scaling d_c from the laboratory to the field is a long-standing and nontrivial problem, largely due to uncertainty as to what it physically represents (e.g., Dieterich, 1981; Griffith & Prakash, 2015; Marone & Kilgore, 1993; McLaskey & Kilgore, 2013). A relevant observation is that following the 10 μm/s run-in, at least 0.6 mm of sliding at the plate rate is required before the laboratory SSEs begin to occur. This might suggest that the spontaneous partial locking leading up to the laboratory SSEs requires attainment of a steady-state microstructure or surface roughness. We speculate that this microstructure or roughness could be characterized by a specific d_c value (e.g., Candela & Brodsky, 2016). As seen in equation (4), smaller d_c favors instability by increasing K_c. Although the evolution of d_c may play a significant role, it is subject to difficulties in scaling and will need to be addressed in a future study.

We also note that other processes not replicated in our experiments may play a role in contributing to relocking processes observed between natural SSEs from cGPS. For example, temporal variations in fluid pressure in the fault zone due to fault-valve behavior (Sibson, 1990) during the SSE cycle could influence the timing of relocking following the SSE. Other natural processes occurring within the fault zone, such as silica dissolution, diffusion, and precipitation (Fisher & Brantley, 2014), or pressure solution (Rutter, 1983; Yasuhara et al., 2005) may also influence the relocking phase observed geodetically. Relocking, and temporal

variations in locking rate observed geodetically could also be explained by the development of force chains between clasts in the mélange/shear zone of plate boundary faults (e.g., Beall et al., 2019).

6.3. Implications for Hikurangi SSE Environment

Our laboratory SSEs exhibit overall depth-increasing trends in parameters such as stress drop, peak slip velocity, event duration, slip, and slip per patch length (Figures 4 and 6). This is consistent with critical stiffness theory which predicts greater instability, and hence larger events, with increasing effective normal stress (equations (4) and (5)). However, projecting these quantities to the depths at which Hikurangi SSEs are observed does not match the observations. An intriguing exception can be seen for the peak slip velocity, where the projections from our laboratory data match the observed peak slip velocities for deep SSEs in the southern Hikurangi margin (Figure 6). One interpretation is that the effective stress conditions at these depths are reasonably close to the 5 MPa/km we assume and that the frictional behavior is accurately captured in our experiments (requiring near-lithostatic fluid pressure), although coincidence cannot be ruled out.

The quantities which show the largest difference between the observations and the laboratory projections are the duration, slip and D/r. One obvious explanation for the inconsistency in duration and slip is the limited slip in laboratory experiments due to the small size of the samples, for which r is 12.7 mm. The difference in D/r is more difficult to explain, because it is a normalized value, showing that even though the slip in our laboratory experiments is small relative to natural SSEs, the slip per patch size is roughly 3 orders of magnitude larger than that of the natural SSEs. Scaling from the laboratory to nature is an issue (e.g., McLaskey & Kilgore, 2013) because D/r values calculated for the laboratory SSEs use an r value equivalent to, and therefore limited by, the sample radius. One key difference between laboratory and natural SSEs is that the slip distribution in our experiments is essentially a boxcar function, where slip is the same everywhere on the sample but drops to zero at the sample boundaries. Future experiments on larger samples where the slipping patch is allowed to grow without being limited by the small sample size could improve estimates of D/r values for laboratory SSEs.

The small sample size in laboratory experiments also causes difficulty in evaluating the role of heterogeneity, which numerical studies show can be an important factor for SSEs (e.g., Skarbek et al., 2012). In particular, we assume shear moduli of 30 GPa for the deep Hikurangi SSEs and 10 GPa for the shallow SSEs as average values. However, Williams and Wallace (2015, 2018) used recent New Zealand-wide seismic velocity models to incorporate the effects of more realistic heterogeneous elastic properties on SSE slip and slip distribution. They found that that slip (and seismic potency) during shallow Hikurangi SSEs could be underestimated by up to ~40%, in models that assume a uniform, elastic half-space. Assuming that the unloading stiffness during the SSEs is unchanged, this suggests that the natural shallow SSEs stress drops listed in Table 1 may also be underestimated. As applied to our comparisons between extrapolations from laboratory data and natural Hikurangi SSE parameters (Figure 6), considering effects of elastic heterogeneity would reduce the difference between our projections and the shallow Hikurangi stress drops. The difference in the absolute value of slip would increase, but the normalized slip D/r for the shallow Hikurangi SSEs would be closer to the laboratory projections. For the deep Hikurangi SSEs, incorporation of heterogeneous material properties suggests that slip and stress drop are overestimated by elastic half-space models by up to 20% (Williams & Wallace, 2015), and therefore, the effect of using models with uniform elastic properties to obtain stress drop for deep SSEs (Table 2) would be the opposite (but smaller) compared to the effect on the shallow SSEs.

Other considerations that likely have an effect on comparing laboratory and natural SSE parameters include differences in temperature between the shallow and deep SSEs, and limited sample material available for testing. Rabinowitz et al. (2018) found that temperature in the range of the shallow SSEs has little influence on the slip behavior of the Hikurangi sample we study here. However, above temperatures of 110 °C (the limit of their study) we expect temperature to modify rate-and-state friction parameters via diagenesis and low-grade metamorphic processes, and activation of different deformation mechanisms that may operate under different timescales (e.g., Blanpied et al., 1998; den Hartog et al., 2012; Niemeijer & Vissers, 2014).

Although our sample is representative of the majority of the sediment column drilled at Site 1124, it is not yet clear if this interval is representative of the megathrust zone where the SSEs occur. Moreover, our laboratory experiments do not capture the effects of several important factors such as temperature, elevated pore

pressure, specific structure (e.g., microfabric), and spatial heterogeneities in lithology. However, coring of the sedimentary section on the subducting Pacific Plate just seaward of the deformation front, a main active frontal thrust, and the upper portion of the overriding plate was carried out during IODP Expedition 375 (Wallace et al., 2019). Logging-while-drilling data acquired during IODP Expedition 372 will further help characterize the ambient conditions and rock properties at the prism toe and within the incoming sedimentary section (Wallace et al., 2019). The samples and data obtained from these two cruises will be critical to constrain the relationship between laboratory and geodetic observations of SSEs. Observatories installed during these expeditions will also give us tighter constraints on the slip rate characteristics of offshore north Hikurangi SSEs in the future.

7. Summary and Conclusions

We performed ultraslow laboratory friction experiments utilizing plate tectonic driving rates (5 cm/yr), which produced laboratory SSEs. Our laboratory SSEs exhibit some key similarities with natural SSEs observed in the Hikurangi subduction zone offshore the North Island of New Zealand, including the form of the displacement record and the size of the stress drop. Using friction parameters measured from velocity step tests, we find that the critical stiffness criterion for unstable slip (based on the parameter $a - b$) is not satisfied. A similar criterion for stable accelerating slip (based on the parameter b) suggests that SSEs may occur in the nominally "stable" regime, where $K/K_b < \sim 4$. Critical stiffness measured directly from laboratory SSE stress drops appears to be a better predictor of fault behavior than stiffness parameters extracted from velocity-step tests in laboratory experiments.

The laboratory SSEs exhibit increasing stress drop, duration, peak slip velocity, slip velocity increase, and total slip as a function of increasing effective normal stress. We use this dependence on effective normal stress to extrapolate these quantities to the depths of naturally occurring Hikurangi SSEs. Comparing the projections with a comprehensive catalog of SSEs documented at the Hikurangi margin shows that, with the exception of the peak slip velocity of deep southern Hikurangi SSEs, the projections fail to match the observations. This highlights difficulties scaling laboratory experiments to field observations, and that correlation between laboratory and natural SSEs is not completely straightforward. This latter point can be improved by further work using new data and samples from recent scientific drilling in the Hikurangi subduction zone.

Acknowledgments
We thank Nick Beeler for his detailed and helpful comments on an earlier version of this manuscript. This research uses samples and/or data provided by the Ocean Drilling Program (ODP). This work was supported by Deutsche Forschungsgemeinschaft (DFG) via Grants EXC309/FZT15 and by the European Research Council (ERC) under the European Union's Horizon 2020 research and innovation program Grant 714430 to M. Ikari. All data are available on the Pangaea data publisher for earth and environmental science (https://doi.org/10.1594/PANGAEA.910598).

References

Bartlow, N. M., Wallace, L. M., Beavan, R. J., Bannister, S., & Segall, P. (2014). Time-dependent modeling of slow slip events and associated seismicity and tremor at the Hikurangi subduction zone, New Zealand. *Journal of Geophysical Research: Solid Earth*, *119*, 734–753. https://doi.org/10.1002/2013JB010209

Bassett, D., Sutherland, R., & Henrys, S. (2014). Slow wavespeeds and fluid overpressure in a region of shallow geodetic locking and slow slip, Hikurangi subduction margin, New Zealand. *Earth and Planetary Science Letters*, *389*, 1–13. https://doi.org/10.1016/j.epsl.2013.12.021

Beall, A., Fagereng, Å., & Ellis, S. (2019). Strength of strained two-phase mixtures: Application to rapid creep and stress amplification in subduction zone Mélange. *Geophysical Research Letters*, *46*, 169–178. https://doi.org/10.1029/2018GL081252

Bell, R., Sutherland, R., Barker, D. H. N., Henrys, S., Bannister, S., Wallace, L., & Beavan, J. (2010). Seismic reflection character of the Hikurangi subduction interface, New Zealand, in the region of repeated Gisborne slow slip events. *Geophysical Journal International*, *180*, 34–48. https://doi.org/10.1111/j.1365-246X.2009.04401.x

Bhattacharya, P., Rubin, A. M., Bayart, E., Savage, H. M., & Marone, C. (2015). Critical evaluation of state evolution laws in rate and state friction: Fitting large velocity steps in simulated fault gouge with time-, slip- and stress-dependent constitutive laws. *Journal of Geophysical Research: Solid Earth*, *120*, 6365–6385. https://doi.org/10.1002/2015JB012437

Bilek, S. L., & Lay, T. (1999). Rigidity variations with depth along interplate megathrust faults in subduction zones. *Nature*, *400*, 443–446.

Blanpied, M. L., Marone, C. J., Lockner, D. A., Byerlee, J. D., & King, D. P. (1998). Quantitative measure of the variation in fault rheology due to fluid-rock interactions. *Journal of Geophysical Research*, *103*, 9691–9712.

Candela, T., & Brodsky, E. E. (2016). The minimum scale of grooving on faults. *Geology*, *44*, 603–606. https://doi.org/10.1130/G37934.1

Carter, R.M., McCave, I.N., Richter, C., & Carter, L., (1999). Proceedings of the Ocean Drilling Program, Initial Reports, 181: College Station, Texas (Ocean Drilling Program. https://doi.org/10.2973/odp.proc.ir.181.2000

Chapman, J. S., & Melbourne, T. I. (2009). Future Cascadia megathrust rupture delineated by episodic tremor and slip. *Geophysical Research Letters*, *36*, L22301. https://doi.org/10.1029/2009GL040465

Chinnery, M. A. (1969). Theoretical fault models. In K. Kasahara & A. E. Stevens (Eds.), *A symposium on processes in the focal region* (Vol. 37, pp. 211–223). Ottawa, Canada: Publications of the Dominion Observatory, Department of Energy, Mines and Resources, Ottawa.

Cook, N. (1981). Stiff testing machines, stick slip sliding, and the stability of rock deformation. In N. L. Carter, M. Friedman, J. M. Logan, & D. W. Stearns (Eds.), *Mechanical behavior of crustal rocks: The Handin volume*, *Geophysical Monograph Series* (Vol. 24, pp. 93–102). Washington, DC: American Geophysical Union.

den Hartog, S. A. M., Peach, C. J., Matthijs de Winter, D. A., Spiers, C. J., & Shimamoto, T. (2012). Frictional properties of megathrust fault gouges at low sliding velocities: New data on effects of normal stress and temperature. *Journal of Structural Geology*, *38*, 156–171. https://doi.org/10.1016/j.jsg.2011.12.001

Dieterich, J. H. (1972). Time-dependent friction in rocks. *Journal of Geophysical Research*, *77*, 3690–3697.

Dieterich, J. H. (1979). Modeling of rock friction 1. Experimental results and constitutive equations. *Journal of Geophysical Research*, *84*, 2161–2168.

Dieterich, J. H. (1981). Constitutive properties of faults with simulated gouge. In N. L. Carter, M. Friedman, J. M. Logan, & D. W. Stearns (Eds.), *Mechanical behavior of crustal rocks: The Handin volume*, *Geophysical Monograph Series* (Vol. 24, pp. 103–120). Washington, DC: American Geophysical Union.

Dieterich, J. H. (1986). A model for the nucleation of earthquake slip. In S. Das, J. Boatwright, & C. H. Scholz (Eds.), *Earthquake source mechanics*, *Geophysical Monograph Series* (Vol. 37, pp. 37–47). Washington, DC: American Geophysical Union.

Dieterich, J. H. (1992). Earthquake nucleation on faults with rate- and state-dependent strength. *Tectonophysics*, *211*, 115–134.

Dieterich, J. H., & Kilgore, B. D. (1996). Implications of fault constitutive properties for earthquake prediction. *Proceedings of the National Academy of Sciences USA*, *93*, 3787–3794.

Dixon, T. H., Jiang, Y., Malservisi, R., McCaffrey, R., Voss, N., Protti, M., & Gonzalez, V. (2014). Earthquake and tsunami forecasts: Relation of slow slip events to subsequent earthquake rupture. *Proceedings of the National Academy of Sciences USA*, *111*, 17,039–17,044. https://doi.org/10.1073/pnas.1412299111

Doser, D. I., & Webb, T. H. (2003). Source parameters of large historical (1917-1961) earthquakes, North Island, New Zealand. *Geophysical Journal International*, *152*, 795–832.

Douglas, A., Beavan, J., Wallace, L., & Townend, J. (2005). Slow slip on the northern Hikurangi subduction interface, New Zealand. *Geophysical Research Letters*, *32*, L16305. https://doi.org/10.1029/2005GL023607

Ellis, S., Fagereng, A., Barker, D., Henrys, S., Saffer, D., Wallace, L., et al. (2015). Fluid budgets along the northern Hikurangi subduction margin, New Zealand: The effect of a subduction seamount on fluid pressure. *Geophysical Journal International*, *202*, 277–297. https://doi.org/10.1093/gji/ggv127

Fisher, D. M., & Brantley, S. L. (2014). The role of silica redistribution in the evolution of slip instabilities along subduction interfaces: Constraints from the Kodiak accretionary complex, Alaska. *Journal of Structural Geology*, *69*, 395–414.

Geist, E. L., & Bilek, S. L. (2001). Effect of depth-dependent shear modulus on tsunami generation along subduction zones. *Geophysical Research Letters*, *28*, 1315–1318.

Goulty, N. R., & Gilman, R. (1978). Repeated creep events on the San Andreas Fault near Parkfield, California, recorded by a strainmeter array. *Journal of Geophysical Research*, *83*, 5415–5419.

Griffith, W. A., & Prakash, V. (2015). Integrating field observations and fracture mechanics models to constrain seismic source parameters for ancient earthquakes. *Geology*, *43*, 763–766. https://doi.org/10.1130/G36773.1

Gu, J. C., Rice, J. R., Ruina, A. L., & Simon, T. T. (1984). Slip motion and stability of a single degree of freedom elastic system with rate and state dependent friction. *Journal of the Mechanics and Physics of Solids*, *32*(3), 167–196.

Han, J., Vidale, J. E., Houston, H., Chao, K., & Obara, K. (2014). Triggering of tremor and inferred slow slip by small earthquakes at the Nankai subduction zone in southwest Japan. *Geophysical Research Letters*, *41*, 8053–8060. https://doi.org/10.1002/2014GL061898

Harbord, C. W. A., Nielsen, S. B., De Paola, N., & Holdsworth, R. E. (2017). Earthquake nucleation of rough faults. *Geology*, *45*, 931–934. https://doi.org/10.1130/G39181.1

Hawthorne, J. C., & Rubin, A. M. (2013). Laterally propagating slow slip events in a rate and state friction model with a velocity-weakening to velocity-strengthening transition. *Journal of Geophysical Research: Solid Earth*, *118*, 3785–3808. https://doi.org/10.1002/jbrb.50261

Hüpers, A., Torres, M. E., Owari, S., McNeill, L. C., Dugan, B., Henstock, T. J., et al. (2017). Release of mineral-bound water prior to subduction tied to shallow seismogenic slip off Sumatra. *Science*, *356*, 841–844. https://doi.org/10.1126/science.aal3429

Ide, S., Beroza, G. C., Shelly, D. R., & Uchide, T. (2007). A scaling law for slow earthquakes. *Nature*, *447*, 76–79. https://doi.org/10.1038/nature05780

Ihmlé, P. F., & Jordan, T. H. (1994). Teleseismic search for slow precursors to large earthquakes. *Science*, *266*, 1547–1551.

Ikari, M. J., Ito, Y., Ujiie, K., & Kopf, A. J. (2015). Spectrum of slip behaviour in Tohoku fault zone samples at plate tectonic slip speeds. *Nature Geoscience*, *8*, 870–874. https://doi.org/10.1038/ngeo2547

Ikari, M. J., & Kopf, A. J. (2017). Seismic potential of weak, near-surface faults revealed at plate tectonic slip rates. *Science Advances*, *3*, e1701269. https://doi.org/10.1126/sciadv.1701269

Ikari, M. J., Kopf, A. J., Hüpers, A., & Vogt, C. (2018). Lithologic control of frictional strength variation in subduction zone sediment inputs. In G. E. Bebout, D. W. Scholl, R. J. Stern, L. M. Wallace, & P. Agard (Eds.), *Subduction top to bottom 2*, *Geosphere* (Vol. 14, pp. 604–625). https://doi.org/10.1130/GES01546.1

Ikari, M. J., Saffer, D. M., & Marone, C. (2009). Frictional and hydrologic properties of clay-rich fault gouge. *Journal of Geophysical Research*, *114*, B05409. https://doi.org/10.1029/2008JB006089

Ikari, M. J., Trütner, S., Carpenter, B. M., & Kopf, A. J. (2015). Shear behavior of DFDP-1 borehole samples from the Alpine Fault, New Zealand, under a wide range of experimental conditions. *International Journal of Earth Sciences*, *104*, 1523–1535. https://doi.org/10.1007/s00531-014-1115-5

Ito, Y., Hino, R., Kido, M., Fujimoto, H., Osada, Y., Inazu, D., et al. (2013). Episodic slow slip events in the Japan subduction zone before the 2011 Tohoku-Oki earthquake. *Tectonophysics*, *600*, 14–26. https://doi.org/10.1016/j.tecto.2012.08.022

Ito, Y., & Ikari, M. J. (2015). Velocity- and slip-dependent weakening in simulated fault gouge: Implications for multimode fault slip. *Geophysical Research Letters*, *42*, 9247–9254. https://doi.org/10.1002/2015GL06582

Kaneko, Y., Wallace, L., Hamling, I. J., & Gerstenberger, M. C. (2018). Simple physical model for the probability of a subduction-zone earthquake following slow slip events and earthquakes: Application to the Hikurangi megathrust, New Zealand. *Geophysical Research Letters*, *45*, 3932–3941. https://doi.org/10.1029/2018GL077641

Kitajima, H., & Saffer, D. M. (2012). Elevated pore pressure and anomalously low stress in regions of low frequency earthquakes along the Nankai Trough subduction megathrust. *Geophysical Research Letters*, *39*, L23301. https://doi.org/10.1029/2012GL053793

Koulali, A., McClusky, S., Wallace, L., Allgeyer, S., Tregoning, P., D'Anastasio, E., & Benavente, R. (2017). Slow slip events and the 2016 TeAraroa M_w 7.1 earthquake interaction: Northern Hikurangi subduction, New Zealand. *Geophysical Research Letters*, *44*, 8336–8344. https://doi.org/10.1002/2017GL074776

Larson, K. M., Kostoglodov, V., Miyazaki, S., & Santiago, J. A. S. (2007). The 2006 aseismic slow slip event in Guerrero, Mexico: New results from GPS. *Geophysical Research Letters*, *34*, L13309. https://doi.org/10.1029/2007GL029912

Leeman, J. R., Saffer, D. M., Scuderi, M. M., & Marone, C. (2016). Laboratory observations of slow earthquakes and the spectrum of tectonic fault slip modes. *Nature Communications*, *7*, 11104. https://doi.org/10.1038/ncomms11104

Linde, A. T., Suyehiro, K., Miura, K., Sacks, I. S., & Takagi, A. (1988). Episodic aseismic earthquake precursors. *Nature*, *334*, 513–515.

Liu, Y., & Rice, J. R. (2005). Aseismic slip transients emerge spontaneously in three-dimensional rate and state modeling of subduction earthquake sequences. *Journal of Geophysical Research*, *110*, B08307. https://doi.org/10.1029/2004JB003424

Liu, Y., & Rice, J. R. (2007). Spontaneous and triggered aseismic deformation transients in a subduction fault model. *Journal of Geophysical Research*, *112*, B09404. https://doi.org/10.1029/2007JB004930

Lowry, A. R. (2006). Resonant slow fault slip in subduction zones forced by climatic load stress. *Nature*, *442*, 802–805.

Marone, C. (1998). Laboratory-derived friction laws and their application to seismic faulting. *Annual Review of Earth and Planetary Sciences*, *26*, 643–696.

Marone, C., & Kilgore, B. (1993). Scaling of the critical slip distance for seismic faulting with shear strain in fault zones. *Nature*, *362*, 618–621.

Matsuzawa, T., Hirose, H., Shibazaki, B., & Obara, K. (2010). Modeling short- and long-term slow slip events in the seismic cycle of large subduction earthquakes. *Journal of Geophysical Research*, *115*, B12301. https://doi.org/10.1029/2010B007566

Mazzotti, S., & Adams, J. (2004). Variability of near-term probability for the next great earthquake on the Cascadia subduction zone. *Bulletin of the Seismological Society of America*, *94*, 1954–1959.

McCaffrey, R., Wallace, L. M., & Beavan, J. (2008). Slow slip and frictional transition at low temperature at the Hikurangi subduction zone. *Nature Geoscience*, *1*, 316–320. https://doi.org/10.1038/ngeo178

McLaskey, G. C., & Kilgore, B. D. (2013). Foreshocks during the nucleation of stick-slip instability. *Journal of Geophysical Research: Solid Earth*, *118*, 2982–2997. https://doi.org/10.1002/jgrb.50232

Niemeijer, A. R., & Vissers, R. L. M. (2014). Earthquake rupture propagation inferred from the spatial distribution of fault rock frictional properties. *Earth and Planetary Science Letters*, *396*, 154–164. https://doi.org/10.1016/j.epsl.2014.04.010

Noda, H., Lapusta, N., & Kanamori, H. (2013). Comparison of average stress drop measures for ruptures with heterogeneous stress change and implications for earthquake physics. *Geophysical Journal International*, *193*, 1691–1712. https://doi.org/10.1093/gji/ggt074

Okada, Y. (1992). Internal deformation due to shear and tensile faults in half-space. *Bulletin of the Seismological Society of America*, *82*, 1018–1040.

Peng, Z., & Gomberg, J. (2010). An integrated perspective of the continuum between earthquakes and slow-slip phenomena. *Nature Geoscience*, *3*, 599–607. https://doi.org/10.1038/NGEO940

Rabinowitz, H. S., Savage, H. M., Skarbek, R. M., Ikari, M. J., Carpenter, B. M., & Collettini, C. (2018). Frictional behavior of input sediments to the Hikurangi Trench, New Zealand. *Geochemistry, Geophysics, Geosystems*, *19*, 2973–2990. https://doi.org/10.1029/2018GC007633

Reinen, L. A., & Weeks, J. D. (1993). Determination of rock friction constitutive parameters using an iterative least squares method. *Journal of Geophysical Research*, *98*, 15,937–15,950.

Reyners, M., & Bannister, S. (2007). Earthquakes triggered by slow slip at the plate interface in the Hikurangi subduction zone, New Zealand. *Geophysical Research Letters*, *34*, L14305. https://doi.org/10.1029/2007GL030511

Rice, J. R., & Ruina, A. L. (1983). Stability of steady frictional slipping. *Journal of Applied Mechanics*, *50*, 343–349.

Rubin, A. M. (2008). Episodic slow slip events and rate-and-state friction. *Journal of Geophysical Research*, *113*, B11414. https://doi.org/10.1029/2008JB005642

Ruina, A. L. (1983). Slip instability and state variable friction laws. *Journal of Geophysical Research*, *88*, 10,359–10,370.

Ruiz, S., Metois, M., Fuenzalida, A., Ruiz, J., Leyton, F., Grandin, R., et al. (2014). Intense foreshocks and a slow slip event preceded the 2014 Iquique M_w 8.1 earthquake. *Science*, *345*, 1165–1169. https://doi.org/10.1126/science.1256074

Rutter, E. H. (1983). Pressure solution in nature, theory and experiment. *Journal of the Geological Society of London*, *140*, 725–740.

Sacks, I. S., Linde, A. T., Snoke, J. A., & Suyehiro, S. (1981). A slow earthquake sequence following the Izu-Oshima earthquake of 1978. In D. W. Simpson & P. G. Richareds (Eds.), *Earthquake prediction: An international review*, *Maurice Ewing Series* (Vol. 4, pp. 617–628). Washington, DC: American Geophysical Union.

Sacks, S. I., Suyehiro, S., Linde, A. T., & Snoke, J. A. (1978). Slow earthquakes and stress redistribution. *Nature*, *275*, 599–602.

Saffer, D. M., & Marone, C. (2003). Comparison of smectite- and illite-rich gouge frictional properties: Application to the updip limit of the seismogenic zone along subduction megathrusts. *Earth and Planetary Science Letters*, *215*, 219–235.

Saffer, D. M., & Wallace, L. M. (2015). The frictional, hydrologic, metamorphic and thermal habitat of shallow slow earthquakes. *Nature Geoscience*, *8*, 594–600. https://doi.org/10.1038/NGEO2490

Scholz, C. H. (1998). Earthquakes and friction laws. *Nature*, *391*, 37–42.

Scholz, C. H. (2002). *The mechanics of earthquakes and faulting* (2nd ed.). New York, NY: Cambridge Press.

Scuderi, M. M., Marone, C., Tinti, E., Di Stefano, G., & Collettini, C. (2016). Precursory changes in seismic velocity for the spectrum of earthquake failure modes. *Nature Geoscience*, *9*, 695–700. https://doi.org/10.1038/NGEO2775

Segall, P., Rubin, A. M., Bradley, A. M., & Rice, J. R. (2010). Dilatant strengthening as a mechanism for slow slip events. *Journal of Geophysical Research*, *115*, B12305. https://doi.org/10.1029/2010JB007449

Shibazaki, B., & Iio, Y. (2003). On the physical mechanism of silent slip events along the deeper part of the seismogenic zone. *Geophysical Research Letters*, *30*(9), 1489. https://doi.org/10.1029/2003GL017047

Shibazaki, B., & Shimamoto, T. (2007). Modelling of short-interval silent slip events in deeper subduction interfaces considering the frictional properties at the unstable-stable transition regime. *Geophysical Journal International*, *171*, 191–205. https://doi.org/10.1111/j.1365-246X.2007.03434.x

Sibson, R. H. (1990). Conditions for fault-valve behaviour. *Geological Society, London, Special Publications*, *54*(1), 15–28.

Skarbek, R. M., Rempel, A. W., & Schmidt, D. A. (2012). Geologic heterogeneity can produce aseismic slip transients. *Geophysical Research Letters*, *39*, L21306. https://doi.org/10.1029/2012GL053762

Trippetta, F., Carpenter, B. M., Mollo, S., Scuderi, M. M., Scarlato, P., & Collettini, C. (2017). Physical and transport property variations within carbonate-bearing fault zones: Insights from the Monte Maggio Fault (central Italy). *Geochemistry, Geophysics, Geosystems*, *18*, 4027–4042. https://doi.org/10.1002/2017GC007097

Underwood, M. B. (2007). Sediment inputs to subduction zone: Why lithostratigraphy and clay mineralogy matter. In T. H. Dixon & J. C. Moore (Eds.), *The Seismogenic Zone of Subduction Thrust Faults* (pp. 42–85). New York: Columbia University Press.

Vogt, C., Lauterjung, J., & Fischer, R. (2002). Investigation of the clay fraction (< 2 μm) of the Clay Minerals Society reference clays. *Clays and Clay Minerals*, *50*(3), 388–400.

Wallace, L. M., Bartlow, N., Hamling, I., & Frye, B. (2014). Quake clamps down on slow slip. *Geophysical Research Letters*, *41*, 8840–8846. https://doi.org/10.1002/2014GL062367

Wallace, L. M., & Beavan, J. (2006). A large slow slip event on the central Hikurangi subduction interface beneath the Manawatu region, North Island, New Zealand. *Geophysical Research Letters*, *33*, L11301. https://doi.org/10.1029/2006/GL026009

Wallace, L. M., & Beavan, J. (2010). Diverse slow slip behavior at the Hikurangi subduction margin, New Zealand. *Journal of Geophysical Research*, *115*, B12402. https://doi.org/10.1029/2010JB007717

Wallace, L. M., Beavan, J., Bannister, S., & Williams, C. (2012). Simulataneous long-term and short-term slow slip events at the Hikurangi subduction margin, New Zealand: Implications for processes that control slow slip event occurrence, duration, and migration. *Journal of Geophysical Research*, *117*, B11402. https://doi.org/10.1029/2012JB009489

Wallace, L. M., Beavan, J., McCaffrey, R., & Darby, D. (2004). Subduction zone coupling and tectonic block rotations in the North Island, New Zealand. *Journal of Geophysical Research*, *109*, B12406. https://doi.org/10.1029/2004JB003241

Wallace, L. M., & Eberhart-Phillips, D. (2013). Newly observed, deep slow slip events at the central Hikurangi margin, New Zealand: Implications for downdip variability of slow slip and tremor, and relationship to seismic structure. *Geophysical Research Letters*, *40*, 5393–5398. https://doi.org/10.1002/2013GL057682

Wallace, L. M., Hreinsdóttir, S., Ellis, S., Hamling, I., D'Anastasio, E., & Denys, P. (2018). Triggered slow slip and afterslip on the southern Hikurangi subduction zone following the Kaikoura earthquake. *Geophysical Research Letters*, *45*, 4710–4718. https://doi.org/10.1002/2018GL077385

Wallace, L. M., Kaneko, Y., Hreinsdóttir, S., Hamling, I., Peng, Z., Bartlow, N., et al. (2017). Large-scale dynamic triggering of shallow slow slip enhanced by overlying sedimentary wedge. *Nature Geoscience*, *10*, 765–770. https://doi.org/10.1038/NGEO3021

Wallace, L. M., Reyners, M., Cochran, U., & Bannister, S. (2009). Characterizing the seismogenic zone of a major plate boundary subduction thrust: Hikurangi Margin, New Zealand. *Geochemistry, Geophysics, Geosystems*, *10*, Q10006. https://doi.org/10.1029/2009GC002610

Wallace, L. M., Saffer, D. M., Barnes, P. M., Pecher, I. A., Petronotis, K. E., LeVay, L. J., & the Expedition 372/375 Scientists (2019). Hikurangi subduction margin coring, logging, and observatories. Proceedings of the International Ocean Discovery Program, 372B/375: College Station, TX (International Ocean Discovery Program). https://doi.org/10.14379/iodp.proc.372B375.2019

Wallace, L. M., Webb, S. C., Ito, Y., Mochizuki, K., Hino, R., Henrys, S., et al. (2016). Slow slip near the trench at the Hikurangi subduction zone, New Zealand. *Science*, *352*, 701–704. https://doi.org/10.1126/science.aaf2349

Wech, A. G., & Creager, K. C. (2011). A continuum of stress, strength and slip in the Cascadia subduction zone. *Nature Geoscience*, *4*, 624–628. https://doi.org/10.1038/NGEO1215

Williams, C. A., & Wallace, L. M. (2015). Effects of material property variations on slip estimates for shallow subduction interface slow-slip events. *Geophysical Research Letters*, *42*, 1113–1121. https://doi.org/10.1002/2014GL062505

Williams, C. A., & Wallace, L. M. (2018). The impact of realistic elastic properties on inversions of shallow subduction interface slow slip events using seafloor geodetic data. *Geophysical Research Letters*, *45*, 7462–7470. https://doi.org/10.1029/2018GL078042

Yasuhara, H., Marone, C., & Elsworth, D. (2005). Fault zone restrengthening and frictional healing: The role of pressure solution. *Journal of Geophysical Research*, *110*, B06310. https://doi.org/10.1029/2004JB003327